Available online at www.sciencedirect.com

ScienceDirect

Ceramics International 40 (2014) 16627–16634

CERAMICS INTERNATIONAL

www.elsevier.com/locate/ceramint

Synthesis by a chemical method and characterization of $CaZrO_3$ powders: Potential application as humidity sensors

R.S. André[a], S.M. Zanetti[b,*], J.A. Varela[b], E. Longo[b]

[a]LIEC/CMDMC, DQ, Universidade Federal de S. Carlos, CEP 13565-905 São Carlos-SP, Brazil
[b]LIEC/INCT, IQ, Universidade Estadual Paulista, P.O. Box 355, CEP 14801-907 Araraquara-SP, Brazil

Received 24 June 2014; received in revised form 6 August 2014; accepted 6 August 2014
Available online 13 August 2014

Abstract

$CaZrO_3$ stoichiometric and non-stoichiometric (CaO- and ZrO_2-excess) powders were synthesized by a chemical method which is based on polymeric precursors. The mesoporous material was characterized using X-ray diffraction (XRD), Raman spectrometry, field emission gun scanning electron microscopy (FE-SEM) and N_2 adsorption–desorption measurements. The humidity sensing properties were evaluated by using an inductance, capacitance and resistance analyzer. The results revealed that all samples responded well to the humidity by showing a change in resistance values; however, hysteresis mean values in the 25–70% relative humidity (RH) range were higher than that of 5%. The CaO-excess sample sensitivity calculated in the 10–85% RH range was 3261. Complex impedance measurements indicated that the improved sample sensitivities can be attributed to their mesoporous structure along with hetero-junctions formed by second phases. Sample resistances varied by about three orders of magnitude in the RH range. These results demonstrate the great potential of CZO samples for use in the development of new humidity sensors.
© 2014 Elsevier Ltd and Techna Group S.r.l. All rights reserved.

Keywords: $CaZrO_3$; Calcium zirconate; Chemical method; Humidity sensor

1. Introduction

There is a growing interest in nanostructured ceramic materials because of their properties which are different and very often superior to conventional material properties. The surface effect role is enhanced in nanostructured materials due to a substantial increase in the fraction of surface atoms which cause property enhancement including quantum confinement in semiconductors, surface plasmon resonance in metals and superparamagnetism in magnetic materials [1].

Ceramic materials which belong to the perovskite family with a general formula of ABO_3 exhibit different magnetic or electric properties such as ferromagnetism or superconductivity [2]. Among the perovskite compounds, $CaZrO_3$ (CZO) (also known as lakargiite) possesses an orthorhombic structure of slightly deformed [ZrO_6] octahedra and [CaO_8]. $CaZrO_3$ is a refractory compound which undergoes polymorph transformation from orthorhombic-$CaZrO_3$ to cubic-$CaZrO_3$ at 1750 °C and melts at 2340 °C [3]; in nature, it has been identified only in Russia in 2008.

CZO is a potential candidate for use in mechanical filters, coatings and in electrical applications such as resonators and capacitors [3]. In addition, studies with $CaZrO_3$ as sensors for monitoring oxygen, humidity and hydrogen have been conducted. According to Gonenli et al. [4], undoped $CaZrO_3$ ceramics are *p*-type semiconductors in air; when doped with a small excess of ZrO_2 or CaO, they become predominantly oxygen-ion conductors.

Normally, CZO has been obtained by the conventional solid state reaction (SSR) which involves high temperature thermal treatment of $CaCO_3$ and ZrO_2 followed by milling to reduce the grain size [5–7]. Despite the high temperature treatment

*Corresponding author:. Tel: +55 16 3301 9653
E-mail addresses: zanettism@gmail.com, zanetti@iq.unesp.br (S.M. Zanetti).

http://dx.doi.org/10.1016/j.ceramint.2014.08.023
0272-8842/© 2014 Elsevier Ltd and Techna Group S.r.l. All rights reserved.

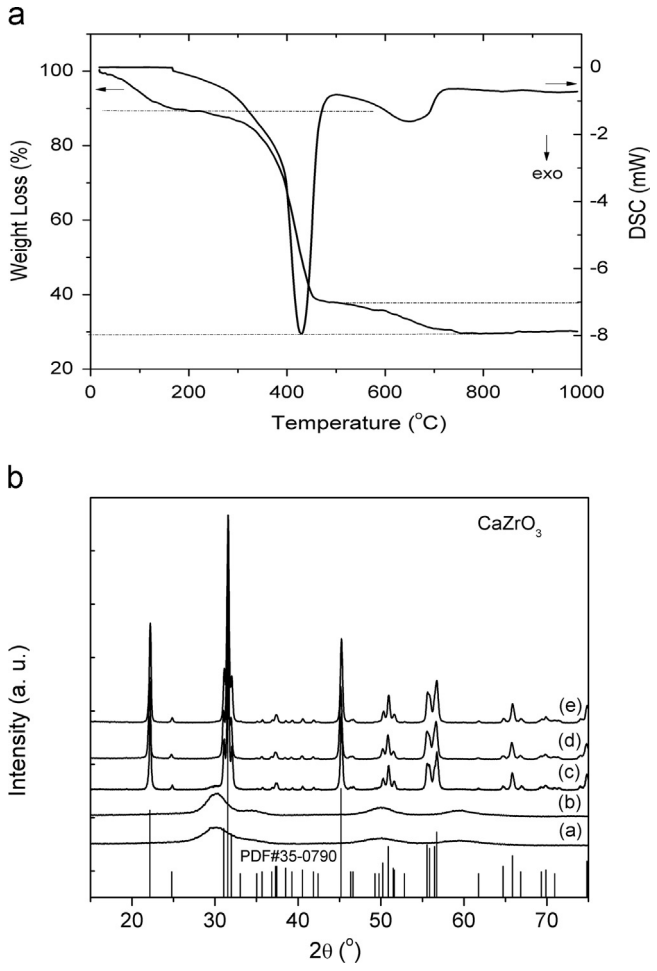

Fig. 1. (a) TGA/DSC measurements for CZO sample heated at 300 °C; and (b) XRD patterns for CZO powders heated at 500 °C (a), 600 °C (b), 700 °C (c), 800 °C (d) and 900 °C (e).

along with the milling process in SSR, the obtained powder is not chemically homogeneous. It exhibits a large particle size and highly agglomerated grains which are detrimental to the sintering process along with the electrical properties [8,9].

To overcome this drawback, alternative synthesis routes have been developed such as combustion synthesis [10,11], a co-precipitation method [12] and chemical solution methods such as, sol–gel [13] among others. Chemical methods facilitate chemically homogenous nanosized grains which are highy desirable to enhance properties.

The aim of the present paper is to obtain stoichiometric CZO, CaO-excess and ZrO_2-excess samples synthesized by the polymeric precursor chemical method (based on the Pechini process). Also, this paper demonstrates CZO powder responses as humidity sensors.

2. Experimental section

Citric acid (CA) was dissolved in water at 60 °C; the zirconium citrate solution was formed by dissolving a stoichiometric amount of $ZrO(NO_3)_2 \cdot nH_2O$ into the CA aqueous solution in a CA:Zr molar ratio equal to 6. After the zirconium citrate solution became homogeneous and translucent, $CaCO_3$ (as a salt) was added in a stoichiometric amount to obtain $CaZrO_3$, $CaZr_{1.2}O_3$ and $Ca_{1.2}ZrO_3$; the samples were identified as CZO, CZO:Zr and CZO:Ca, respectively. Then ethylene glycol (EG) was added to the citrate solution in a 2:3 (CA:EG) mass ratio. The entire process was carried out at 60 °C under continuous stirring to obtain a homogeneous transparent yellow resin. The temperature was increased to 75 °C until a highly viscous liquid was obtained. The resins were heat treated at 300 °C for 4 h to eliminate organic material which was followed by treatment at 900 °C for 2 h for phase crystallization.

TGA measurements were carried out in a Netzsch STA 409C equipment from room temperature to 1000 °C at a 10 °C min^{-1} rate, under a 30 mL min^{-1} O_2 flux.

The samples were characterized by XRD in a Rigaku DMax 2500PC diffractometer using Cu Kα radiation (40 kV and 150 mA) and Raman spectrometry. Raman spectra were recorded on a RFS/100/S Bruker Fourier transform Raman (FT-Raman) spectrometer with a 1064 nm excitation wavelength using a Nd:YAG laser; the spectral resolution used was 4 cm^{-1}.

Morphology and size characterizations were performed by FEG-SEM (Supra 35-VP, Carl Zeiss); all measurements were taken at room temperature.

The powder surface area was measured by the BET method using a Micromeritics ASAP 2010 instrument with nitrogen as the adsorption gas. The mean grain size, D_{BET}, was calculated by the equation:

$$D_{BET} = \frac{6000}{\rho S_{BET}}, \quad (1)$$

where D_{BET} is the mean grain size (nm), ρ is the theoretical density of $CaZrO_3$ samples and S_{BET} is the BET surface area (m^2 g^{-1}).

Pellets of CZO powders were heat-treated at 900 °C, and sensing elements were formed with silver paste as electrodes. The electrical resistance as a function of RH measurements was carried out in a controlled climatic chamber (BT2001, 10–85% RH, at 25 °C) to observe their response as humidity sensors. Impedance measurements were performed from 10 Hz to 1 MHz with an AUTOLAB (PGSTAT with a FRA2 system using NOVA software). Controlled humidity environments were obtained with saturated salt solutions of LiCl, $MgCl_2$, NaBr, NaCl, KCl and K_2SO_4 in a closed glass vessel at room temperature which yielded 11%, 29%, 56%, 75%, 85% and 97% RH, respectively. Samples were soaked for at least 60 min in each humidity level before the electrical measurement.

3. Results and discussion

TGA result for CZO sample (see Fig. 1a) shows a weight loss of 51.7% from 200 °C to 500 °C, due to the elimination of most part of the organics, a small loss of 7.4% from 500 °C to 800 °C, due to the total elimination of organics. Above 800 °C no loss is observed. Simultaneous DSC measurement reveals two exothermic events: a sharp peak centered at 429 °C

attributed to the elimination of organics and a broad peak around 655 °C which can be assigned to the elimination of organics along with the crystallization of the CZO phase.

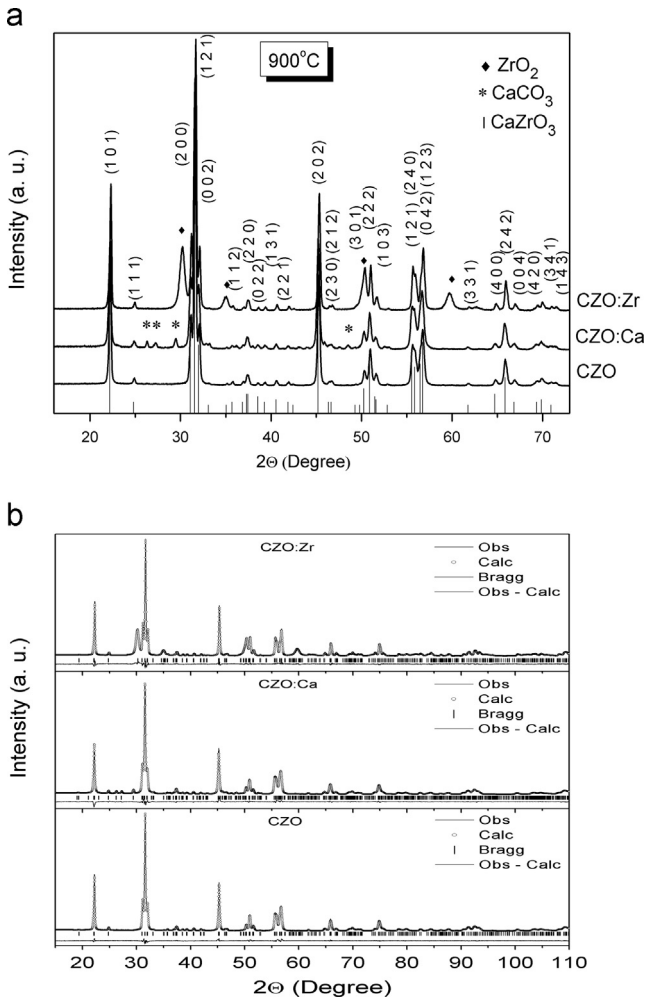

Fig. 2. (a) XRD patterns for CZO powders heated at 900 °C; and (b) structural refinement for CZO samples.

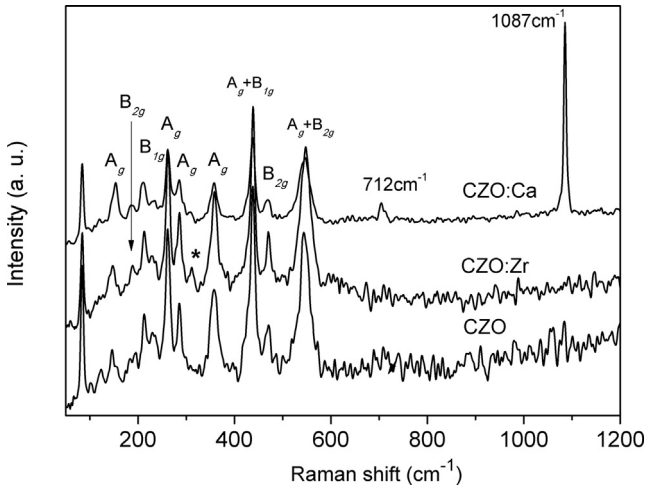

Fig. 3. Raman spectra of CZO samples.

In order to follow the crystallization process, X-ray diffraction were carried out in samples heat-treated at temperatures from 500 °C to 900 °C (see Fig. 1b). At 500 °C and 600 °C the sample is amorphous while at 700 °C a crystallized CZO phase

Table 1
Raman frequencies of the $CaZrO_3$ phase observed in this study as compared to Orera's study [15] and related modes.

This work (γ cm^{-1})	Ref. [15] (γ cm^{-1})	Related mode
84	–	
147	145	(A_g) lattice soft mode
195	190	(B_{2g}) Zr–O bending
212	212	(B_{2g}) Zr–O bending
227	227	(B_{1g} or B_{3g}) Zr–O bending
237	234	(B_{2g}) Zr–O bending
261	262.5	(A_g) Zr–O bending
285	286.5	(A_g) Zr–O bending
–	305	(B_{1g} or B_{3g}) torsion mode
357	358	(A_g) torsion mode
–	418	(B_{2g}) torsion mode
438	439	(A_g+B_{1g}) torsion mode
471	469	(B_{2g}) Zr–O stretching
544	543	(A_g+B_{2g}) Zr–O stretching
–	547	(B_{1g} or B_{3g}) Zr–O stretching

Table 2
Surface area and mean grain size measured by the BET method.

Sample	Theoretical density (g cm^{-3})	Surface area (m^2 g^{-1})	D_{BET} (nm)
CZO:Zr	4.45	6.9	195
CZO	4.78	9.2	136
CZO:Ca	3.23	13.1	142

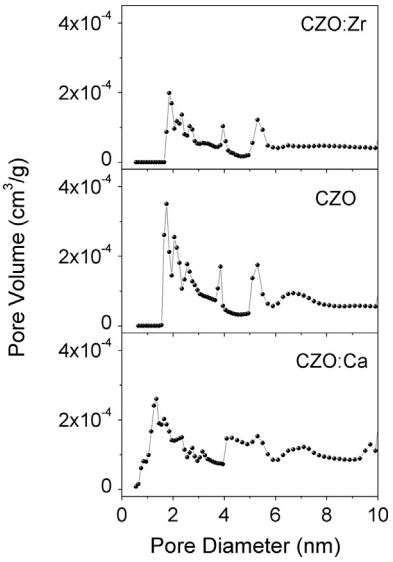

Fig. 4. Pore diameter distribution of CZO samples obtained from BET data.

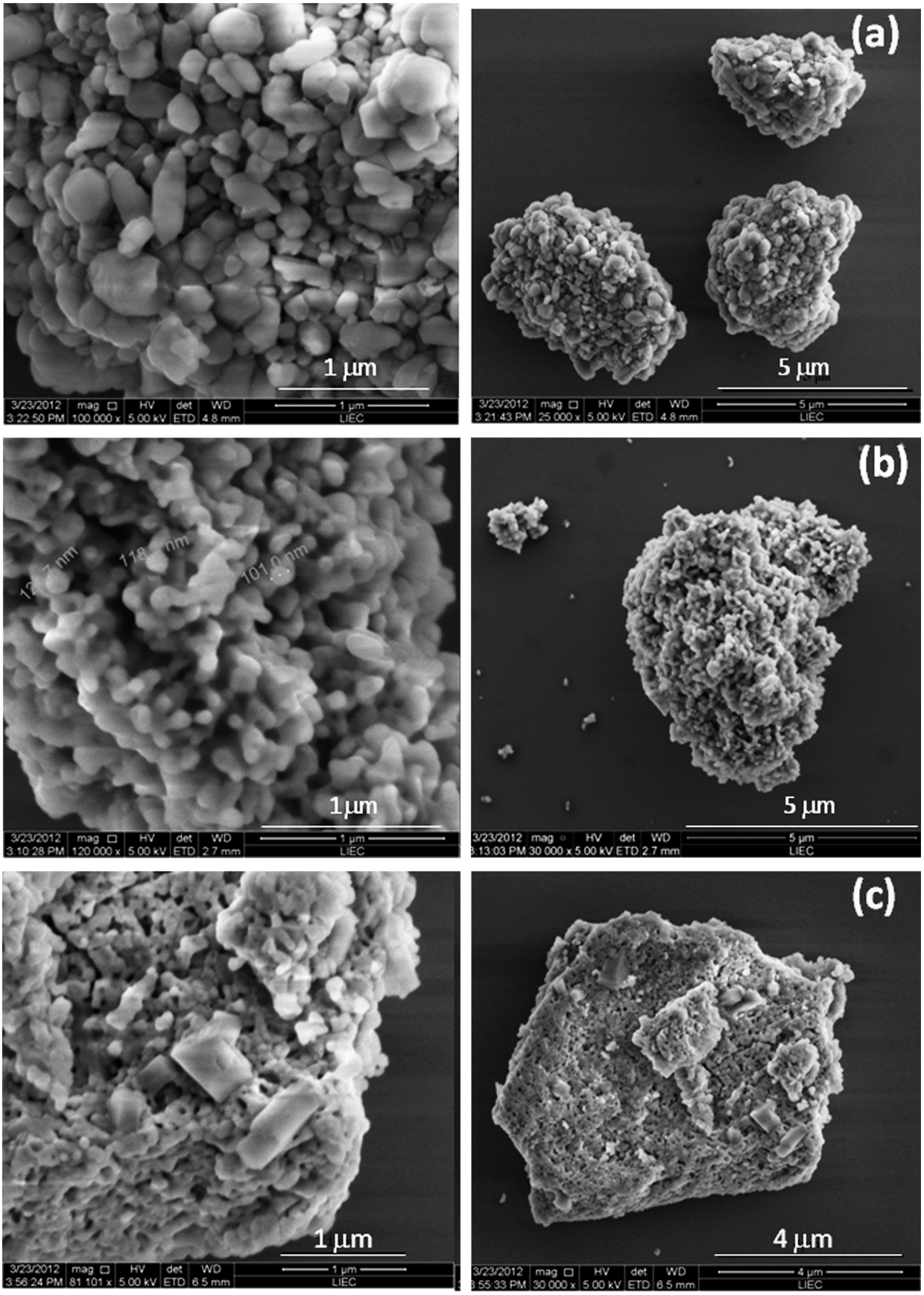

Fig. 5. Micrograph images of FEG for synthesized powders: (a) CZO:Zr, (b) CZO, and (c) CZO:Ca.

is observed along with a small peak of the amorphous phase at 30° (2θ), which confirms the DSC results.

Fig. 2a illustrates that all the samples are crystalline at 900 °C; the $CaZrO_3$ phase with an orthorhombic structure and a space group *of Pnmc* (PDF 35-0790) is also displayed.

Rietveld refinement (see Fig. 2b) reveals that the CZO sample contained 100% of the $CaZrO_3$ stoichiometric phase. For the CZO:Zr sample, the structural refinement denotes that 74.3% is the $CaZrO_3$ stoichiometric phase while 25.7% is ZrO_2 with a tetragonal structure which belongs to a space group of *P*42/*nmc* (PDF 50-1089) as the secondary phase. The CZO:Ca sample diffraction pattern exhibits small peaks that could be attributed to $CaCO_3$ (PDF 5-586 and 41-1475). The structural refinement identifies that 83.5% is the $CaZrO_3$ stoichiometric phase while 16.5% is the $CaCO_3$ phase (12.1% in an aragonite form and 4.4% in a calcite form).

XRD results agree with the report of Dudek et al. [13] who observed that even a minimum of Zr excess results in a significant amount of cubic zirconia whereas the same amount of Ca excess results in a number of weak lines attributed to the $CaCO_3$ phase.

Fig. 3 shows Raman spectra of CZO samples; Raman active modes are localized in smaller wavelengths as suggested by Levin et al. [14]. A number of modes cannot be detected due to their lower polarizabilities or because some predicted modes are hidden behind other intense bands. Raman active modes related to the $CaZrO_3$ phase are shown in Table 1 and are compared with Orera's work Ref. [15].

Raman active modes characteristic of $CaCO_3$ are observed at 712 cm^{-1} and 1087 cm^{-1} for the CZO:Ca sample which confirms that a second phase exists [16]. According to Li et al. [17], Raman bands at 149, 269 and 312 cm^{-1} are assigned to the ZrO_2 tetragonal phase. Although, in CZO:Zr spectra only the band at 312 cm^{-1} is clearly observed, one can infer that ZrO_2 is the secondary phase as XRD results already illustrate.

The BET analysis showed a specific surface area of 6.9, 9.2 and 13.1 m^2g^{-1} for samples CZO:Zr, CZO and CZO:Ca, respectively. The average grain size was calculated by Eq. (1), and the results are displayed in Table 2 which shows that the sample with excess ZrO_2 (CZO:Zr) exhibits a larger mean grain size than both the stoichiometric (CZO) and CaO-excess (CZO:Ca) samples.

The pore size was extracted from nitrogen adsorption isotherms by the BET method. The results show a very similar pore size profile for CZO:Zr and CZO samples with pores around 1.8–2.6 nm whereas the CZO:Ca sample shows pores around 0.8–1.4 nm (see Fig. 4).

The particle morphology was observed by FEG-SEM; all samples show quite agglomerated particles composed of nano-sized grains. Fig. 5 illustrates that the stoichiometric CZO (see Fig. 5b) has a homogeneous porous microstructure of quite spherical grains. On the other hand, CZO:Zr and the CZO:Ca have a microstructure of grains with different morphologies which is probably due to secondary phases. Note that the sample with a ZrO_2 phase (see Fig. 5a) has larger grains whereas the sample with a $CaCO_3$ phase (see Fig. 5c) is composed of highly agglomerated smaller spherical grains along with squared grains. These results are in agreement with results observed by BET measurements (see Table 2).

As mentioned earlier, CZO is a promising material as a ceramic sensor for humidity measurement. To verify the performance of CZO as a humidity sensor, the samples were exposed to a controlled humidity chamber, and their electric resistance response to the variation in humidity was measured. Measurements were carried out using 1 V AC and 1 kHz frequency, and the results are shown in Fig. 6. All samples responded well to humidity by showing a change in the resistance values of four orders of magnitude. All samples exhibited about $10^6\,\Omega$ resistance at low relative humidity RH = 10% which decreased exponentially with an increase in RH.

Humidity sensitivity is defined as $S = R_d/R_h$ where R_d and R_h are resistance values taken at 10% RH and at a particular RH, respectively. The greater the value of S, the higher is the sensitivity of the sample to moisture. Table 3 verifies that S values calculated in the 10–85% RH range for CZO:Zr, CZO and CZO:Ca samples were 3261, 1351 and 1296, respectively.

The humidity hysteresis was evaluated by the difference in logarithmic impedance between adsorption and desorption processes in the 25–70% RH range [18]. Hysteresis mean values of CZO:Zr and CZO samples were 5% and 8%, respectively; CZO:Ca sample value was 11%, which is quite

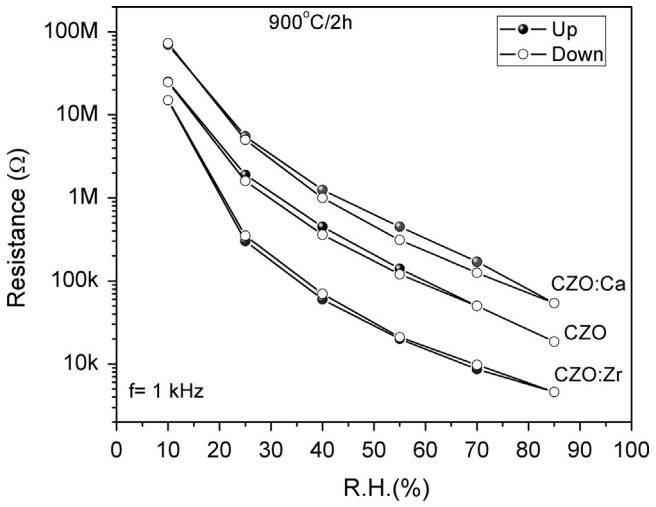

Fig. 6. Electrical response of CZO samples as a function of the relative humidity.

Table 3
Calculated sensitivity values for CZO samples.

Sample	CZO:Zr	CZO	CZO:Ca
10% RH	1	1	1
25% RH	50	13	13
40% RH	250	56	56
55% RH	750	179	156
70% RH	1744	500	412
85% RH	3261	1351	1296

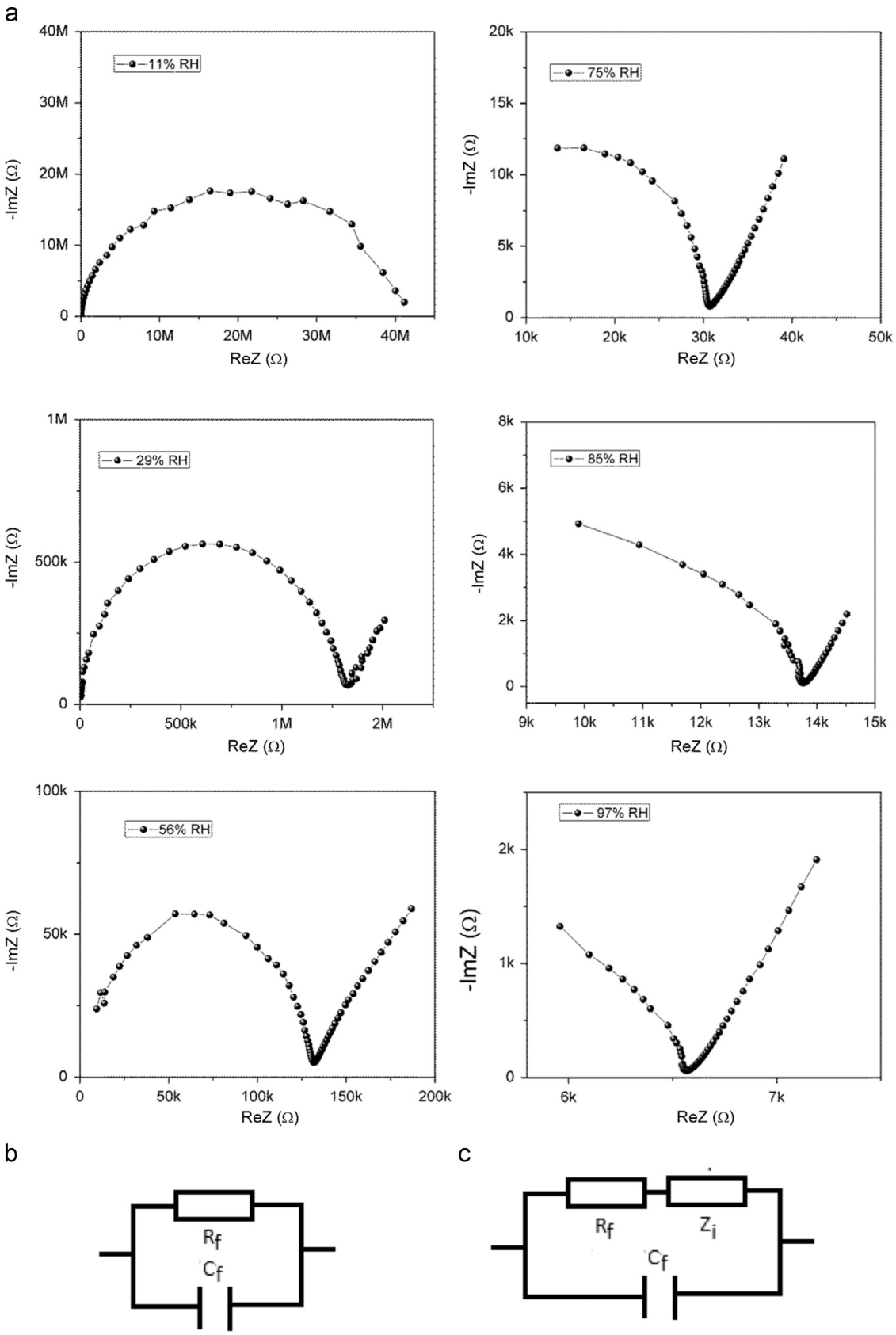

Fig. 7. (a) Complex impedance plots of stoichiometric CZO at different RH levels. An equivalent circuit of complex impedance plots: (a) low humidity level; (b) high humidity level.

high. The higher hysteresis CZO:Ca sample values can be attributed to a smaller pore diameter (see Fig. 4) which can retard water molecule desorption.

To analyze the humidity-sensing mechanism of CZO samples, the complex impedance was studied. The frequency range varied from 10 Hz to 1 MHz, and the RH ranged from 11% to 97% RH at room temperature. Measurements revealed the same profile for all samples; however, only the CZO sample results are shown in Fig. 7a. When RH is low (11%, 29%), a semi-circle is observed. The sensing mechanism represented by the semi-circle plot could be modeled by an equivalent parallel circuit of a resistor and a capacitor [19] (see Fig. 7b). As the RH increases, the semi-circle at a high frequency range is accompanied by a line after the semi-circle at the low frequency range. The curve of the line connected with the semi-circle represents another type of sensing mechanism which takes into account electrode–ceramics interfaces (see Fig. 7c). Hence, two different humidity-sensing mechanisms can be observed at low and high RH levels. At low RH due to the low water content, there was movement of the H^+ on the ceramics surface which caused the extremely high impedance (around 40 MΩ at 11% RH). According to the Grotthuss chain reaction [20], at a high RH, the adsorbed water could dissolve ions (H_3O^+) which could interact with the opposite charge resulting in a sharp decrease of the impedance (around 1.5 MΩ at 29% RH and 30 kΩ, at 75% RH).

The good humidity sensing characteristics of CZO sensors described here could be attributed to their mesoporous structure which permits the water molecule (in addition to being adsorbed on the surface) to also enter the pore and be adsorbed on pore walls. Also, the second phase can provide hetero-junctions which create positive and negative charges on the surface and can readily attract water molecules to improve the sensitivity.

These calcium zirconate hetero-junctions could be thought of in terms of charge carriers clusters such as $[ZrO_5V_O]$, $[ZrO_5V_O^{\bullet\bullet}]$, $[CaO_{11}V_O^{\bullet}]$ and $[CaO_{11}V_O^{\bullet\bullet}]$. These clusters can interact with the water molecule according to the equations below:

$$[ZrO_5V_O^{\bullet}] + OH_2 \rightarrow [ZrO_5V_O^{\bullet}]\ldots OH_{2\ (ads)} \quad (2)$$

$$[ZrO_5V_O^{\bullet}]\ldots OH_{2\ (ads)} \rightarrow [ZrO_5V_O^{x}]\ldots OH^*_{(ads)} + H^{\bullet} \quad (3)$$

$$[ZrO_5V_O^{\bullet\bullet}] + OH_2 \rightarrow [ZrO_5V_O^{\bullet\bullet}]\ldots OH_{2\ (ads)} \quad (4)$$

$$[ZrO_5V_O^{\bullet\bullet}]\ldots OH_{2\ (ads)} \rightarrow [ZrO_5V_O^{\bullet}]\ldots OH^* + H^{\bullet} \quad (5)$$

where OH* is a hydroxyl radical. In the literatures [21,22], the same mechanism is attributed to photocatalytic activities of $SrWO_4$ and $SrTiO_3$ which interact with O_2 molecules.

In addition, calcium clusters may also have a role which is similar to the role reported above as follows:

$$[CaO_{11}V_O^{\bullet}] + OH_2 \rightarrow [CaO_{11}V_O^{\bullet}]\ldots OH_{2\ (ads)} \quad (6)$$

$$[CaO_{11}V_O^{\bullet}]\ldots OH_2 \rightarrow [CaO_{11}V_O^{x}]\ldots OH^* + H^{\bullet} \quad (7)$$

$$[CaO_{11}V_O^{\bullet\bullet}] + OH_2 \rightarrow [CaO_{11}V_O^{\bullet\bullet}]\ldots OH_{2\ (ads)} \quad (8)$$

$$[CaO_{11}V_O^{\bullet\bullet}]\ldots OH_{2\ (ads)} \rightarrow [CaO_{11}V_O^{x}]\ldots OH^* + H^{\bullet} \quad (9)$$

These equations illustrate the mechanism of CZO sample sensing properties due to second phase interfaces which increase or reduce its conductivity. Variations in clusters concentration (CaO and ZrO_2) influence adsorption mechanisms with the formation of OH* radicals and hydrogen radicals, $H^{\bullet}$, which alter the sample conductivity and consequently its electrical resistance. Furthermore, a second phase can change interfaces by influencing the growth of particles, the surface area and the distribution and density of defects. As a result, the CZO sample impedance continuously decreases by more than three orders of magnitude as compared with the initial impedance.

4. Conclusion

Stoichiometric $CaZrO_3$ (CZO) and non-stoichiometric (CaO- and ZrO_2-excess, CZO:Ca and CZO:Zr, respectively) were successfully synthesized by a chemical method and were characterized as humidity sensors. The stoichiometric composition is a $CaZrO_3$ single phase compound while the non-stoichiometric compositions show secondary phases such as ZrO_2 and $CaCO_3$. Electrical measurements showed that all samples responded as humidity sensors with high sensitivity values (calculated at 85% RH) of 3261, 1351 and 1296 for. CZO:Zr, CZO and CZO:Ca samples, respectively. However, hysteresis mean values of CZO:Zr, CZO and CZO:Ca samples in the 25–70% RH range were 5%, 8% and 11%, respectively which is quite high. Thus there is clearly considerable room for improvement of the microstructure in order to reach hysteresis values required for humidity sensors. Complex impedance analysis attested to the good humidity sensing characteristics which could be attributed to a sensor mesoporous structure along with the hetero-junctions provided by the second phase to improve the sensitivity. Sample resistances varied about three orders of magnitude in the RH range. These results demonstrate the great potential of CZO samples for use in the development of new humidity sensors.

Acknowledgments

The authors acknowledge the financial support of the Brazilian research financing institutions: CNPq (Proc. 573636/2008-7, 150591/2011-0), FAPESP (Proc. 2013/07296-2), INCTMN (Proc. 2008/57872-1) and CAPES.

References

[1] M.H. Zhou, A. Ahmad, Sol–gel processing of In-doped CaZrO3 solid electrolyte and the impedimetric sensing characteristics of humidity and hydrogen, Sens. Actuators B 129 (2008) 285–291.

[2] M. Tarrida, H. Larguem, M. Madon, Structural investigations of (Ca,Sr) ZrO_3 and Ca(Sn,Zr)O_3 perovskite compounds, Phys. Chem. Miner. 36 (2009) 403–413.

[3] C.S. Prasanth, et al., Synthesis, characterization and microwave dielectric properties of nanocrystalline $CaZrO_3$ ceramics, J. Alloys Compd. 464 (2008) 306–309.
[4] I.E. Gonenli, A.C. Tas, Chemical synthesis of pure and Gd-doped $CaZrO_3$ powders, J. Eur. Ceram. Soc. 19 (1999) 2563–2567.
[5] M. Pollet, M. Daturi, S. Marinel, Vibrational spectroscopy study of the lattice defects in $CaZrO_3$ ceramics, J. Eur. Ceram. Soc. 24 (2004) 1805–1809.
[6] S.C. Hwang, G.M. Choi, The mixed ionic and electronic conductivity of $CaZrO_3$ with cation nonstoichiometry and oxygen partial pressure, Solid State Ion. 179 (2008) 1042–1045.
[7] P. Stoch, et al., Crystal structure and ab initio calculations of $CaZrO_3$, J. Eur. Ceram. Soc. 32 (2012) 665–670.
[8] M. Dudek, M.M. Bucko, Electrical properties of stoichiometric and non-stoichiometric calcium zirconate, Solid State Ion. 157 (2003) 183–187.
[9] S.C. Hwang, G.M. Choi, The effect of cation nonstoichiometry on the electrical conductivity of acceptor-doped $CaZrO_3$, Solid State Ion. 177 (2006) 3099–3103.
[10] R. Ianos, P. Barvinschi, Solution combustion synthesis of calcium zirconate, $CaZrO_3$, powders, J. Solid State Chem. 183 (2010) 491–496.
[11] K. Boobalan, A. Varun, R. Vijayaraghavan, K. Chidambaram, U. Kamachi Mudali, Facile, scalable synthesis of nanocrystalline calcium zirconate by the solution combustion method, Ceram. Int. 40 (2014) 5781–5786.
[12] V. Krishnan, J.W. Fergus, Effects of dispersant addition on the synthesis of indium-doped calcium zirconate by co-precipitation techniques, J. Mater. Sci. 42 (2007) 6117–6122.
[13] M. Dudek, E. Drozdz-Ciesla, Some observations on synthesis and electrolytic properties of nonstoichiometric calcium zirconate, J. Alloys Compd. 475 (2009) 846–854.
[14] I. Levin, et al., Local structures and Raman spectra in the $Ca(Zr,Ti)O_3$ perovskite solid solutions, Chem. Mater. 18 (2006) 854–860.
[15] V.M. Orera, et al., Vibrational spectroscopy of $CaZrO_3$ single crystals, J. Phys. Condens. Matter 10 (1998) 7501–7510.
[16] S. Akyuz, et al., Pigment analyses of a portrait and paint box of Turkish artist Feyhaman Duran (1886–1970): the EDXRF, FT-IR and micro Raman spectroscopic studies, Spectrochim. Acta 89 (2012) 74–81.
[17] C. Li, M.J. Li, UV Raman spectroscopic study on the phase transformation of ZrO_2, Y_2O_3–ZrO_2 and SO_4^{2-}/ZrO_2, J. Raman Spectrosc. 33 (2002) 301–308.
[18] Y. Kim, et al., Capacitive humidity sensor design based on anodic aluminum oxide, Sens. Actuators B 141 (2009) 441–446.
[19] J. Wang, Q. Lin, R. Zhou, B. Xu, Humidity sensors based on composite material of nano-$BaTiO_3$ and polymer RMX, Sens. Actuators B 81 (2002) 33–394.
[20] N. Agmon, The Grotthuss mechanism, Chem. Phys. Lett. 244 (1995) 456–462.
[21] L.S. Cavalcante, et al., Growth mechanism and photocatalytic properties of $SrWO_4$ microcrystals synthesized by injection of ions into a hot aqueous solution, Adv. Powder Technol. 24 (2013) 344–353.
[22] L.F. Silva, et al., Long-range and short-range structures of cube-like shape $SrTiO_3$ powders: microwave-assisted hydrothermal synthesis and photocatalytic activity, Phys. Chem. Chem. Phys. 15 (2013) 12386.